THE ASTROPHYSICAL JOURNAL SUPPLEMENT SERIES, 126:501–516, 2000 February

THE ACCURACY, CONSISTENCY, AND SPEED OF AN ELECTRON-POSITRON EQUATION OF STATE BASED ON TABLE INTERPOLATION OF THE HELMHOLTZ FREE ENERGY

F. X. TIMMES[1] AND F. DOUGLAS SWESTY[2]
Received 1999 May 14; accepted 1999 August 30

ABSTRACT

An electron-positron equation of state based on table interpolation of the Helmholtz free energy is developed and analyzed. The interpolation scheme guarantees perfect thermodynamic consistency, independent of the interpolating function. The choice of a biquintic Hermite polynomial as the interpolating function results in accurately reproducing the underlying Helmholtz free energy data in the table, and yields derivatives of the pressure, specific entropy, and specific internal energy which are smooth and continuous. The execution speed—evaluated across several different machine architectures, compiler options, and modes of operation—suggests that the Helmholtz equation of state routine is faster than any of the five equation of state routines surveyed by Timmes & Arnett. When an optimal balance of accuracy, thermodynamic consistency, and speed is desirable then the tabular Helmholtz equation of state is an excellent choice, particularly for multidimensional models of stellar phenomena.

Subject headings: equation of state — hydrodynamics — methods: numerical — stars: general

1. INTRODUCTION

Models of stellar events usually require the relationship between various thermodynamic properties over a large span of temperatures, densities, and compositions. Stellar equation of state (henceforth EOS) routines are used for the thermodynamic conditions found in models of stellar evolution, supernovae, novae, and X-ray bursts, so the EOS must be accurate in regions where the electrons and positrons have a speed arbitrarily close to the causal limits and an arbitrary degree of degeneracy. With over 10^9 calls to the EOS being common in two- and three-dimensional hydrodynamic models of stellar phenomena, it is very desirable to have an electron-positron EOS that is as efficient as possible and yet accurately represents the relevant physics.

Direct evaluation of the electron-positron physics in the EOS is usually accurate enough and thermodynamically consistent, but it is often overly time consuming within the context of a two- or three-dimensional model. Tabular equations of state for the electron-positron plasma are usually efficient enough for multidimensional models, but bring about their own set of difficulties with regard to accuracy and consistency. These difficulties include the need for accurate interpolations, the need for a temperature-density grid which is dense enough to provide sufficient resolution of the thermodynamic variables, and the need for the interpolated values to be thermodynamically consistent with each other (i.e., satisfy the Maxwell relations). In many circumstances the number of points in the temperature-density grid can always be made large enough to keep the accuracy and level of thermodynamic inconsistency at an acceptable level, although in some cases the memory or cache requirements can begin to deteriorate the efficiency of using a tabular EOS. It is our intent to minimize the amount of table tuning.

The purpose of this paper is to present a method of evaluating electron-positron equation of state tables which maintains fidelity to the underlying thermodynamic data with a modest temperature-density grid, and which guarantees thermodynamic consistency of the interpolated values.

In § 2 we discuss the mechanics of the method. The accuracy, thermodynamic consistency, and speed of the resulting EOS routines are analyzed in § 3. A summary of our findings is given in § 4, and in the Appendix we list a FORTRAN routine which implements the method.

2. IMPLEMENTATION

2.1. *Assuring Thermodynamic Consistency*

Let isotope i have Z_i protons and A_i nucleons (protons + neutrons). Let the aggregate total of isotope i have a number density n_i (in cm^{-3}) in material with a temperature T (in K) and a mass density ρ (in g cm^{-3}). Define the dimensionless mass fraction of isotope i as $X_i = \rho_i/\rho = n_i A_i/(\rho N_{\rm A})$, where $N_{\rm A}$ is Avogadro's number. The mean number of nucleons per isotope is defined as $\overline{A} = (\sum X_i/A_i)^{-1}$, the mean charge per isotope is defined as $\overline{Z} = \overline{A} \sum Z_i X_i/A_i$, and the number of electrons per baryon is defined as $Y_e = \overline{Z}/\overline{A}$. Under these conditions, let the material have a scalar pressure P (in ergs cm^{-3}), a specific internal energy E (in ergs g^{-1}), and a specific entropy S (in ergs g^{-1} K^{-1}).

The first law of thermodynamics

$$dE = TdS + \frac{P}{\rho^2}\, d\rho \tag{1}$$

[1] Center on Astrophysical Thermonuclear Flashes, University of Chicago, 933 East 56th Street, Chicago, IL 60637.
[2] Department of Physics and Astronomy, SUNY at Stony Brook, Stony Brook, NY 11794.

is an exact differential, which requires that the thermodynamic relations

$$P = \rho^2 \left.\frac{\partial E}{\partial \rho}\right|_T + T \left.\frac{\partial P}{\partial T}\right|_\rho , \tag{2}$$

$$\left.\frac{\partial E}{\partial T}\right|_\rho = T \left.\frac{\partial S}{\partial T}\right|_\rho , \tag{3}$$

$$-\left.\frac{\partial S}{\partial \rho}\right|_T = \frac{1}{\rho^2} \left.\frac{\partial P}{\partial T}\right|_\rho , \tag{4}$$

be satisfied. An equation of state is thermodynamically consistent if all three of these identities are true. Thermodynamic inconsistency may manifest itself in the unphysical buildup (or decay) of the entropy (or temperature) during numerical simulations of what should be an adiabatic flow. Models of events which are sensitive to the entropy (e.g., core-collapse supernovae) may suffer inaccuracies if thermodynamic consistency is significantly violated over a sufficient number of time steps (Swesty 1996).

When the temperature and density are the natural thermodynamic variables to use, the appropriate thermodynamic potential is the Helmholtz free energy

$$F = E - TS, \qquad dF = -SdT + \frac{P}{\rho^2} d\rho . \tag{5}$$

With the pressure defined as

$$P = \rho^2 \left.\frac{\partial F}{\partial \rho}\right|_T , \tag{6}$$

the first of the Maxwell relations (eq. 2) is automatically satisfied, as substitution of equation (5) into equation (6) demonstrates. With the entropy defined as

$$S = -\left.\frac{\partial F}{\partial T}\right|_\rho , \tag{7}$$

the second of the Maxwell relations (eq. 3) is automatically satisfied, as substitution of equation (5) into equation (7) demonstrates. The requirement that the mixed partial derivatives commute

$$\frac{\partial^2 F}{\partial T \partial \rho} = \frac{\partial^2 F}{\partial \rho \partial T} \tag{8}$$

ensures that the third of the thermodynamic identity (eq. 4) is satisfied, as substitution of equation (5) into equation (8) shows.

Consider *any* interpolating function for the Helmholtz free energy $F(\rho, T)$ which satisfies equation (8). Thermodynamic consistency is guaranteed as long as equation (6) is used first to evaluate the pressure, equation (7) is used second to evaluate the entropy, and finally equation (5) is used to evaluate the internal energy (Swesty 1996). In fact, this procedure is almost too robust! The interpolated values may be horribly inaccurate but they will be thermodynamically consistent. Having presented this method that guarantees thermodynamic consistency, the next task to consider is the construction of an interpolating function that retains fidelity to the underlying data.

2.2. *Construction of the Biquintic Polynomials*

Given any interpolating function for the Helmholtz free energy, the pressure, entropy, and internal energy are given by derivatives of the interpolating function. The derivatives of the pressure, entropy, and internal energy, are in turn given by the second derivatives of the interpolating function. One also wants the derivatives of the pressure, entropy, and internal energy to be continuous across the table grid points, not for any thermodynamic reasons, but for convergence of the Newton-Raphson iterative schemes that are invariably present in explicit or implicit time integrations of the fluid equations. From these general considerations, the minimum order of an interpolating polynomial that will suffice is a quartic. For the reasons given below, the minimum order of the interpolating polynomial is actually a quintic. With this choice of an interpolating function, the Helmholtz free energy is given by a quintic polynomial in both the density and temperature table directions. The pressure, entropy, and internal energy are given by a quartic polynomials, and the derivatives of the pressure, entropy, and internal energy are given by cubic polynomials.

Suppose one wants to define a function on the interval $[x_i, x_{i+1}]$ that has the following properties:

$$\begin{aligned} f(x_i) &= C_1, \qquad f(x_{i+1}) = C_2 , \\ f'(x_i) &= C_3, \qquad f'(x_{i+1}) = C_4 , \end{aligned} \tag{9}$$

where the C_i are arbitrary constants. The lowest order polynomial that could satisfy these four conditions is a cubic:

$$f(x) = A + Bx + Cx^2 + Dx^3 . \tag{10}$$

The conditions of equation (9) determine the coefficients A, B, C, and D in terms of the C_i. The two polynomials multiplying the resultant C_i are the cubic Hermite basis functions (e.g., Davis 1963, p. 37):

$$\psi_0(z) = 2z^3 - 3z^2 + 1 ,$$
$$\psi_1(z) = z^3 - 2z^2 + z , \tag{11}$$

where

$$z = \frac{x - x_i}{x_{i+1} - x_i} , \tag{12}$$

and the interpolating cubic Hermite polynomial is

$$H_3(z) = f_i \psi_0(z) + f_{i+1} \psi_0(1 - z) + \left.\frac{\partial f}{\partial x}\right|_i (x_{i+1} - x_i)\psi_1(z) - \left.\frac{\partial f}{\partial x}\right|_{i+1} (x_{i+1} - x_i)\psi_1(1 - z) . \tag{13}$$

To use the cubic Hermite interpolant one must tabulate the function $f(x)$ and its first derivative df/dx at the grid points. In return for this investment, the values of the function and its first derivative are reproduced exactly at the grid points. In addition, the values of the function and the first derivative change continuously as the interpolating point moves from one grid cell to the next. Note the derivative of cubic Hermite polynomial is given by the derivative of the basis functions in equation (11).

The cubic Hermite basis functions are extended from one dimension to two dimensions by interpolating each of the basis functions in the second dimension. An example of the resulting bicubic interpolation is given by Press et al. (1996). Unfortunately, bicubic interpolation is insufficient for a Helmholtz free energy based equation of state because the derivatives of the pressure, entropy, and internal energy would be given by piecewise linear functions, which would be discontinuous as the interpolating point moves from one grid cell to the next. These discontinuities would cause nonconvergence in the root-finding schemes that are invariably present in stellar hydrodynamic programs. To gain continuity of the pressure, entropy, and internal energy derivatives one must go to the next order Hermite polynomial.

Imposing conditions on the second derivative of a function on the interval $[x_i, x_{i+1}]$

$$f(x_i) = C_1 , \qquad f(x_{i+1}) = C_2 ,$$
$$f'(x_i) = C_3 , \qquad f'(x_{i+1}) = C_4 ,$$
$$f''(x_i) = C_5 , \qquad f''(x_{i+1}) = C_6 , \tag{14}$$

and applying the same techniques as above, yields the three quintic Hermite basis functions:

$$\psi_0(z) = -6z^5 + 15z^4 - 10z^3 + 1 ,$$
$$\psi_1(z) = -3z^5 + 8z^4 - 6z^3 + z ,$$
$$\psi_2(z) = \tfrac{1}{2}(-z^5 + 3z^4 - 3z^3 + z^2) . \tag{15}$$

In this case the interpolating quintic Hermite polynomial (Davis 1963, page 37) is

$$H_5(z) = f_i \psi_0(z) + f_{i+1} \psi_0(1 - z) + \left.\frac{\partial f}{\partial x}\right|_i (x_{i+1} - x_i)\psi_1(z) - \left.\frac{\partial f}{\partial x}\right|_{i+1} (x_{i+1} - x_i)\psi_1(1 - z)$$
$$+ \left.\frac{\partial^2 f}{\partial x^2}\right|_i (x_{i+1} - x_i)^2\psi_2(z) + \left.\frac{\partial^2 f}{\partial x^2}\right|_{i+1} (x_{i+1} - x_i)^2\psi_2(1 - z) . \tag{16}$$

The one-dimensional quintic polynomial is extended to two dimensions by interpolating each of the basis functions in the second dimension. The resulting biquintic interpolation function (Swesty 1996) for the density and temperature rectangle bounded by $\rho_i \le \rho < \rho_{i+1}$ and $T_i \le T < T_{i+1}$ is given by

$$H_5(\rho, T) = F_{i,j}\psi_0(x)\psi_0(y) + F_{i+1,j}\psi_0(1 - x)\psi_0(y) + F_{i,j+1}\psi_0(x)\psi_0(1 - y) + F_{i+1,j+1}\psi_0(1 - x)\psi_0(1 - y)$$
$$+ \left.\frac{\partial F}{\partial T}\right|_{i,j} (T_{j+1} - T_j)\psi_1(x)\psi_0(y) - \left.\frac{\partial F}{\partial T}\right|_{i+1,j} (T_{j+1} - T_j)\psi_1(1 - x)\psi_0(y) + \left.\frac{\partial F}{\partial T}\right|_{i,j+1} (T_{j+1} - T_j)\psi_1(x)\psi_0(1 - y)$$
$$- \left.\frac{\partial F}{\partial T}\right|_{i+1,j+1} (T_{j+1} - T_j)\psi_1(1 - x)\psi_0(1 - y) + \left.\frac{\partial^2 F}{\partial T^2}\right|_{i,j} (T_{j+1} - T_j)^2\psi_2(x)\psi_0(y) + \left.\frac{\partial^2 F}{\partial T^2}\right|_{i+1,j} (T_{j+1} - T_j)^2\psi_2(1 - x)\psi_0(y)$$
$$+ \left.\frac{\partial^2 F}{\partial T^2}\right|_{i,j+1} (T_{j+1} - T_j)^2\psi_2(x)\psi_0(1 - y) + \left.\frac{\partial^2 F}{\partial T^2}\right|_{i+1,j+1} (T_{j+1} - T_j)^2\psi_2(1 - x)\psi_0(1 - y) + \left.\frac{\partial F}{\partial \rho}\right|_{i,j} (\rho_{i+1} - \rho_i)\psi_0(x)\psi_1(y)$$
$$+ \left.\frac{\partial F}{\partial \rho}\right|_{i+1,j} (\rho_{i+1} - \rho_i)\psi_0(1 - x)\psi_1(y) - \left.\frac{\partial F}{\partial \rho}\right|_{i,j+1} (\rho_{i+1} - \rho_i)\psi_0(x)\psi_1(1 - y) - \left.\frac{\partial F}{\partial \rho}\right|_{i+1,j+1} (\rho_{i+1} - \rho_i)\psi_0(1 - x)\psi_1(1 - y)$$
$$+ \left.\frac{\partial^2 F}{\partial \rho^2}\right|_{i,j} (\rho_{i+1} - \rho_i)^2\psi_0(x)\psi_2(y) + \left.\frac{\partial^2 F}{\partial \rho^2}\right|_{i+1,j} (\rho_{i+1} - \rho_i)^2\psi_0(1 - x)\psi_2(y) + \left.\frac{\partial^2 F}{\partial \rho^2}\right|_{i,j+1} (\rho_{i+1} - \rho_i)^2\psi_0(x)\psi_2(1 - y)$$

$$
\begin{aligned}
&+ \frac{\partial^2 F}{\partial \rho^2}\bigg|_{i+1,j+1} (\rho_{i+1}-\rho_i)^2\psi_0(1-x)\psi_2(1-y) + \frac{\partial^2 F}{\partial T \partial \rho^2}\bigg|_{i,j} (T_{j+1}-T_j)(\rho_{i+1}-\rho_i)\psi_1(x)\psi_1(y) \\
&- \frac{\partial^2 F}{\partial T \partial \rho}\bigg|_{i+1,j} (T_{j+1}-T_j)(\rho_{i+1}-\rho_i)\psi_1(1-x)\psi_1(y) - \frac{\partial^2 F}{\partial T \partial \rho^2}\bigg|_{i,j+1} (T_{j+1}-T_j)(\rho_{i+1}-\rho_i)\psi_1(x)\psi_1(1-y) \\
&+ \frac{\partial^2 F}{\partial T \partial \rho}\bigg|_{i+1,j+1} (T_{j+1}-T_j)(\rho_{i+1}-\rho_i)\psi_1(1-x)\psi_1(1-y) + \frac{\partial^3 F}{\partial T^2 \partial \rho}\bigg|_{i,j} (T_{j+1}-T_j)^2(\rho_{i+1}-\rho_i)\psi_2(x)\psi_1(y) \\
&+ \frac{\partial^3 F}{\partial T^2 \partial \rho}\bigg|_{i+1,j} (T_{j+1}-T_j)^2(\rho_{i+1}-\rho_i)\psi_2(1-x)\psi_1(y) - \frac{\partial^3 F}{\partial T^2 \partial \rho}\bigg|_{i,j+1} (T_{j+1}-T_j)^2(\rho_{i+1}-\rho_i)\psi_2(x)\psi_1(1-y) \\
&- \frac{\partial^3 F}{\partial T^2 \partial \rho}\bigg|_{i+1,j+1} (T_{j+1}-T_j)^2(\rho_{i+1}-\rho_i)\psi_2(1-x)\psi_1(1-y) + \frac{\partial^3 F}{\partial \rho^2 \partial T}\bigg|_{i,j} (T_{j+1}-T_j)(\rho_{i+1}-\rho_i)^2\psi_1(x)\psi_2(y) \\
&- \frac{\partial^3 F}{\partial \rho^2 \partial T}\bigg|_{i+1,j} (T_{j+1}-T_j)^2(\rho_{i+1}-\rho_i)^2\psi_1(1-x)\psi_2(y) + \frac{\partial^3 F}{\partial \rho^2 \partial T}\bigg|_{i,j+1} (T_{j+1}-T_j)(\rho_{i+1}-\rho_i)^2\psi_1(x)\psi_2(1-y) \\
&- \frac{\partial^3 F}{\partial \rho^2 \partial T}\bigg|_{i+1,j+1} (T_{j+1}-T_j)(\rho_{i+1}-\rho_i)^2\psi_1(1-x)\psi_2(1-y) + \frac{\partial^4 F}{\partial T^2 \partial \rho^2}\bigg|_{i,j} (T_{j+1}-T_j)^2(\rho_{i+1}-\rho_i)^2\psi_2(x)\psi_2(y) \\
&+ \frac{\partial^4 F}{\partial T^2 \partial \rho^2}\bigg|_{i+1,j} (T_{j+1}-T_j)^2(\rho_{i+1}-\rho_i)^2\psi_2(1-x)\psi_2(y) + \frac{\partial^4 F}{\partial T^2 \partial \rho^2}\bigg|_{i,j+1} (T_{j+1}-T_j)^2(\rho_{i+1}-\rho_i)^2\psi_2(x)\psi_2(1-y) \\
&+ \frac{\partial^4 F}{\partial T^2 \partial \rho^2}\bigg|_{i+1,j+1} (T_{j+1}-T_j)^2(\rho_{i+1}-\rho_i)^2\psi_2(1-x)\psi_2(1-y) \,, \qquad (17)
\end{aligned}
$$

where in analogy with equation (12),

$$x = \frac{\rho - \rho_i}{\rho_{i+1} - \rho_i} \,, \qquad y = \frac{T - T_j}{T_{i+1} - T_i} \,. \qquad (18)$$

Despite the rather ungainly appearance of the 36 terms in equation (17), the repetitive patterns in the structure of the equation allow for a concise evaluation (see the Appendix).

To use the biquintic Hermite interpolant for a Helmholtz free energy based equation of state, one must tabulate the Helmholtz free energy F and the eight partial derivatives $\partial F/\partial T$, $\partial F/\partial \rho$, $\partial^2 F/\partial T^2$, $\partial^2 F/\partial \rho^2$, $\partial^2 F/\partial T \partial \rho$, $\partial^3 F/\partial T^2 \partial \rho$, $\partial^3 F/\partial \rho^2 \partial T$, $\partial^4 F/\partial T^2 \partial \rho^2$, as a function of density and temperature. In return for this nontrivial investment, the values of the function, first partial derivatives, and second partial derivatives are reproduced exactly at the grid points. The values of the function, and its first and second partial derivatives, change continuously as the interpolating point moves from one grid cell to the next. With equation (17) as the interpolating function, the Helmholtz free energy is given by a biquintic polynomial. The pressure, entropy, and internal energy are given by a biquartic polynomials, and the derivatives of the pressure, entropy, and internal energy are given by bicubic polynomials. Note the partial derivatives of biquintic interpolant are determined by the derivatives of the three basis functions in equation (15).

Fortunately, five of the eight partial derivatives needed to use the biquintic interpolant can usually be formed from the EOS routine which is used to generate the equations:

$$
\begin{aligned}
F &= E - TS \,, \\
\frac{\partial F}{\partial T}\bigg|_\rho &= -S, \qquad \frac{\partial F}{\partial \rho}\bigg|_T = \frac{P}{\rho^2} \,, \\
\frac{\partial^2 F}{\partial T^2}\bigg|_\rho &= -\frac{\partial S}{\partial T}\bigg|_\rho, \qquad \frac{\partial^2 F}{\partial \rho^2}\bigg|_T = \frac{1}{\rho^2}\frac{\partial P}{\partial \rho}\bigg|_T - \frac{2P}{\rho^3} \,, \\
\frac{\partial^2 F}{\partial T \partial \rho} &= -\frac{\partial S}{\partial \rho}\bigg|_T = \frac{\partial^2 F}{\partial T \partial \rho} = \frac{1}{\rho^2}\frac{\partial P}{\partial T}\bigg|_\rho \,. \qquad (19)
\end{aligned}
$$

The third partial derivatives ($\partial^3 F/\partial T^2 \partial \rho$, $\partial^3 F/\partial \rho^2 \partial T$) and the fourth partial derivative ($\partial^4 F/\partial \rho^2 \partial T^2$) are rarely available directly from the EOS routine. However, these third and fourth partial derivatives may be obtained from techniques which produce accurate numerical derivatives. For example, we have obtained good quality third and fourth partial derivatives with the routine DFRIDR from Press et al. (1996). One simply replaces the lines in DFRIDR which implement the first derivative finite difference approximation with the appropriate third and fourth derivative finite difference approximations. Note that the third and fourth order partial derivatives are not necessary to ensure that the interpolant and its partial derivatives obtain the proper values at the grid points, or to insure smoothness across cell boundaries. What the third and fourth partial derivatives do ensure is that the values of $\partial^2 F/\partial T^2$ and $\partial^2 F/\partial \rho^2$ (both of which contain valuable thermodynamic data) remain well behaved in the middle of a cell. Omission of the three "twist" terms can allow the second partial derivatives of the

interpolant to exhibit undesirable oscillations as one moves through the center of a cell. An example where omission of the third and fourth derivatives can cause errant behavior is at temperatures where pair-production starts to dominate the thermodynamic state.

Once a table of the Helmholtz free energy and eight of its partial derivatives has been constructed, then use of equations (5–8) and equation (17) supplies the thermodynamically consistent interpolated values:

$$P = \rho^2 \frac{\partial F}{\partial \rho}, \qquad \left.\frac{\partial P}{\partial T}\right|_\rho = \rho^2 \frac{\partial^2 F}{\partial \rho \partial T}, \qquad \left.\frac{\partial P}{\partial \rho}\right|_T = \rho^2 \frac{\partial^2 F}{\partial \rho^2} + 2\rho \frac{\partial F}{\partial \rho},$$

$$S = -\frac{\partial F}{\partial T}, \qquad \left.\frac{\partial S}{\partial T}\right|_\rho = -\frac{\partial^2 F}{\partial T^2}, \qquad \left.\frac{\partial S}{\partial \rho}\right|_T = -\frac{\partial^2 F}{\partial \rho \partial T},$$

$$E = F + TS, \qquad \left.\frac{\partial E}{\partial T}\right|_\rho = T \frac{\partial S}{\partial T}, \qquad \left.\frac{\partial E}{\partial \rho}\right|_T = \frac{\partial F}{\partial \rho} + T \frac{\partial S}{\partial \rho}. \tag{20}$$

Now in possession of a method which guarantees thermodynamic consistency and a suitable interpolating polynomial, the next task is to construct an accurate electron-positron EOS table. Before doing so, it behooves us to point out that the principle of maximum entropy, $d^2S < 0$, implies an inequality for the intrinsic stability of matter against temperature variations

$$\left.\frac{\partial E}{\partial T}\right|_\rho = C_v \geq 0, \tag{21}$$

and an inequality for thermodynamic stability against density fluctuations (e.g., Reif 1965, chap. 8)

$$\left.\frac{\partial P}{\partial \rho}\right|_T \geq 0. \tag{22}$$

The interpolation scheme presented above does not guarantee that these two stability inequalities are satisfied. It would, of course, be desirable to formulate an interpolation scheme which did ensure thermodynamic stability, as well as ensure thermodynamic consistency. Such an interpolation scheme would appear to require more coefficients than the biquintic scheme described above since all of the coefficients in the biquintic scheme are uniquely determined by imposing smoothness and continuity of the interpolating function, its first partial derivatives, and its second partial derivatives (eq. [17]). Additional constraints appears to require requires additional coefficients. It is presently unclear (to the authors!) how the additional coefficients should be chosen in order to guarantee that certain second partial derivatives of the interpolant (eqs. [21]–[22]) are positive-definite, a subject of active research in shape-preserving interpolation theory (e.g., Späth 1995; Costantini & Manni 1996). For these reasons, the interpolation scheme presented above restricts attention to maintaining accuracy to the underlying data at the grid points, continuity of the thermodynamic variables, and thermodynamic consistency. Thus, it remains necessary with the present scheme to numerically verify that the stability inequalities of equations (21)–(22) are satisfied. Extensive checks of the tabular electron-positron EOS developed in this paper failed to find a single temperature, density, and composition input point where the thermodynamic stability inequalities were violated.

2.3. *Making the Electron-Positron Equation of State Table*

Timmes & Arnett (1999) compared the accuracy, thermodynamic consistency, and execution speed of five different EOS routines that are used in modeling stellar events. The EOS routines examined in their survey encompass one that is exact (for the assumptions imposed) in IEEE 64-bit arithmetic and served as the reference point for the comparisons (the Timmes EOS). The other four EOS routines analyzed were one written by Iben which was designed primarily for evolving models of intermediate- and low-mass stars (Iben, Fujimoto, & MacDonald 1992); one composed by Weaver, Zimmerman, & Woosley (1978) which aims chiefly for evolving models of massive stars; one summarized by Nadyozhin (1974) and explained in detail by Blinnikov et al. (1996, 1998); and one developed by Arnett (1996). The analysis performed in the Timmes & Arnett (1999) survey permits a complete assessment of these five equation of state routines.

The electron-positron Helmholtz free energy table is constructed with the Timmes EOS, which was designed for maximum accuracy and thermodynamic consistency at the expense of speed. Evaluation of the requisite Fermi-Dirac integrals, along with their partial derivatives, are calculated to at least 18 significant figures with the efficient quadrature schemes of Aparicio (1998). That is, the Fermi-Dirac integrals and their derivatives are exact in IEEE 64 bit arithmetic (16 significant figures). Newton-Raphson iteration is used to obtain the chemical potential to at least 15 significant figures. All the partial derivatives of the pressure, entropy, and internal energy are formed analytically, and the 1986 recommended values of the fundamental physical constants (Cohen & Taylor 1987) are used to their published precision.

The table generated from the Timmes EOS stores the electron-positron Helmholtz free energy and the requisite eight partial derivatives to 16 significant figures. The limits of the table were chosen to be $10^{-6} < \rho < 10^{11}$ g cm^{-3} and $10^4 < T < 10^{11}$ K. This range of 17 orders of magnitude in density and 7 orders of magnitude in temperature is large enough to alleviate concerns about exceeding the limits of table with canonical models of stellar phenomena.

It is vital to note that the Helmholtz free energy table is constructed only for the electron-positron plasma, is two-dimensional $F(\rho, T)$, and is made with $\overline{A} = \overline{Z} = 1$ (pure hydrogen). One reason for not including contributions from photons and ions in the table is that these components of the EOS are very simple (assumed in this paper to be blackbody radiation and ideal gas, respectively) and one does not need fancy table look-up schemes to evaluate simple analytical functions. A more

important reason for only constructing an electron-positron EOS table with $Y_e = 1$ is that the two-dimensional table is valid for *any* composition. Separate planes for each Y_e are not necessary (or desirable) since simple multiplication or division by Y_e in the appropriate places gives the desired composition scaling (see Appendix). If photons and ions were included in the table, then this valuable composition independence would be lost, and three-dimensional tables would be necessary. The EOS routine which implements table look-up of the electron-positron contributions, along with the analytic radiation and ion contributions, is termed the Helmholtz EOS.

Three different density-temperature grids were considered in order to assess the accuracy of the biquintic polynomial as a function of the table size. The "nominal grid" consists of 10 points per decade in both the density and temperature. For the density and temperature range under consideration, this means 171 density grid points and 71 temperature grid points. Since each grid point stores nine quantities, the nominal grid has a memory footprint of 0.87 Mbyte in IEEE 488 double precision arithmetic. The "1/4 nominal grid" consists of 5 points per decade in both the density and temperature directions. This grid has 86 density points, 36 temperature points, and a memory footprint of 0.22 Mbyte in IEEE 488 64 bit arithmetic. The "4 times nominal grid" consists of 20 points per decade in both the density and temperature directions. This grid thus has 341 density grid points, 141 temperature grid points, and a memory footprint of 3.4 Mbyte in 64-bit arithmetic.

All the necessary pieces are now in place; a method which assures thermodynamic consistency, a suitable interpolating polynomial, and a electron-positron EOS table with very precise entries. How accurate, how thermodynamically consistent, and how fast the Helmholtz EOS executes is evaluated in the next section.

3. ACCURACY, CONSISTENCY, AND SPEED OF THE HELMHOLTZ EOS

The pressure relative to the (exact) Timmes EOS is shown in Figure 1. The upper panel is for a temperature of 10^8 K, the middle panel for 10^9 K, and the lower panel for 10^{10} K. The y-axis in each panel gives the absolute value of the deviation from the correct answer, while the x-axis gives the mass density. Red curves are for the nominal grid, blue curves for the 1/4 nominal grid, and green curves are for 4 times nominal grid. The error in the pressure made by the 1/4 nominal grid (*blue curves*) is typically about 1% or less, the error committed by using the nominal grid is typically about 1 part in 10^5, while using the 4 × nominal grid produces errors of about 1 part in 10^6. Note that the distribution of the errors is relatively flat; there are no regions where the error is a pronounced maximum or a minimum. All three curves decrease at the smaller densities in the upper panel because ions begin to dominate contributions to the total pressure, and the ion thermodynamics is identical in the Timmes and Helmholtz EOS routines.

The specific internal energy relative to the Timmes EOS, which was used to create the electron-positron table, is shown in Figure 2. The format of the plot is the same as in Figure 1. In general, the error in the specific internal energy is about 1–2

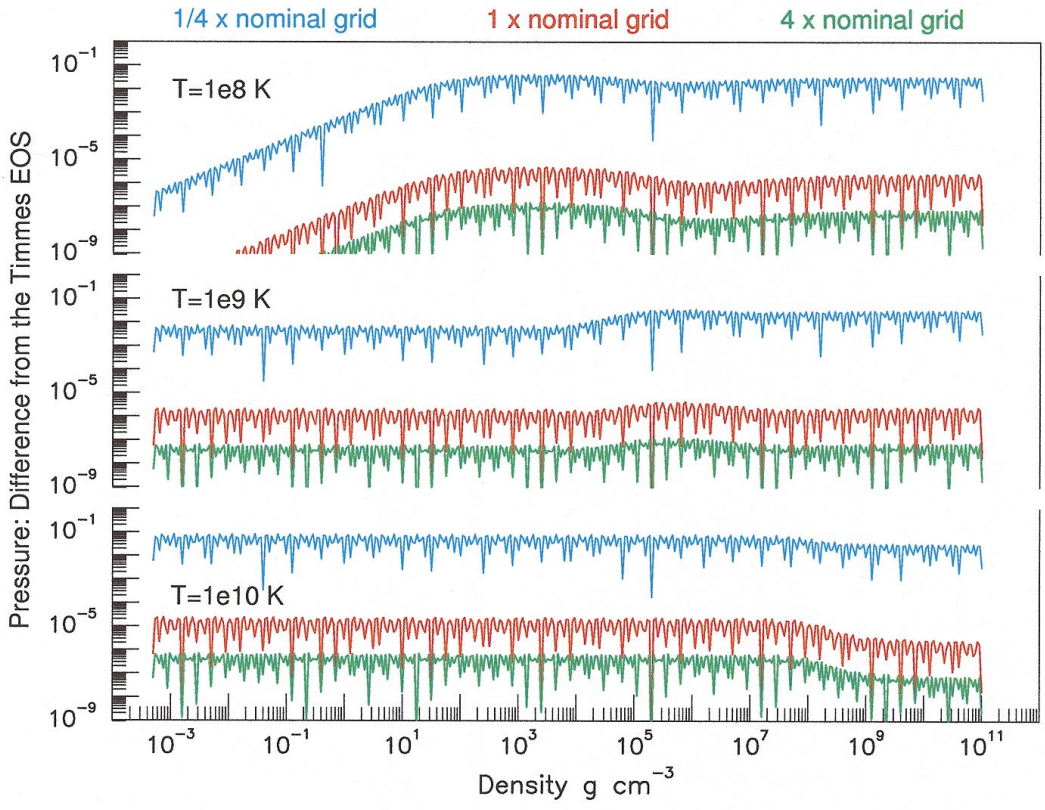

FIG. 1.—Absolute value of the relative difference from the exact Timmes EOS for the scalar pressure. *Top*: 10^8 K; *middle*: 10^9 K; *bottom*: 10^{10} K. The y-axis in each panel gives the modulus of the relative difference from the correct answer, while the x-axis gives the mass density. Red curves are for the nominal grid, blue curves for the 1/4 nominal grid, and green curves are for 4 times nominal grid case.

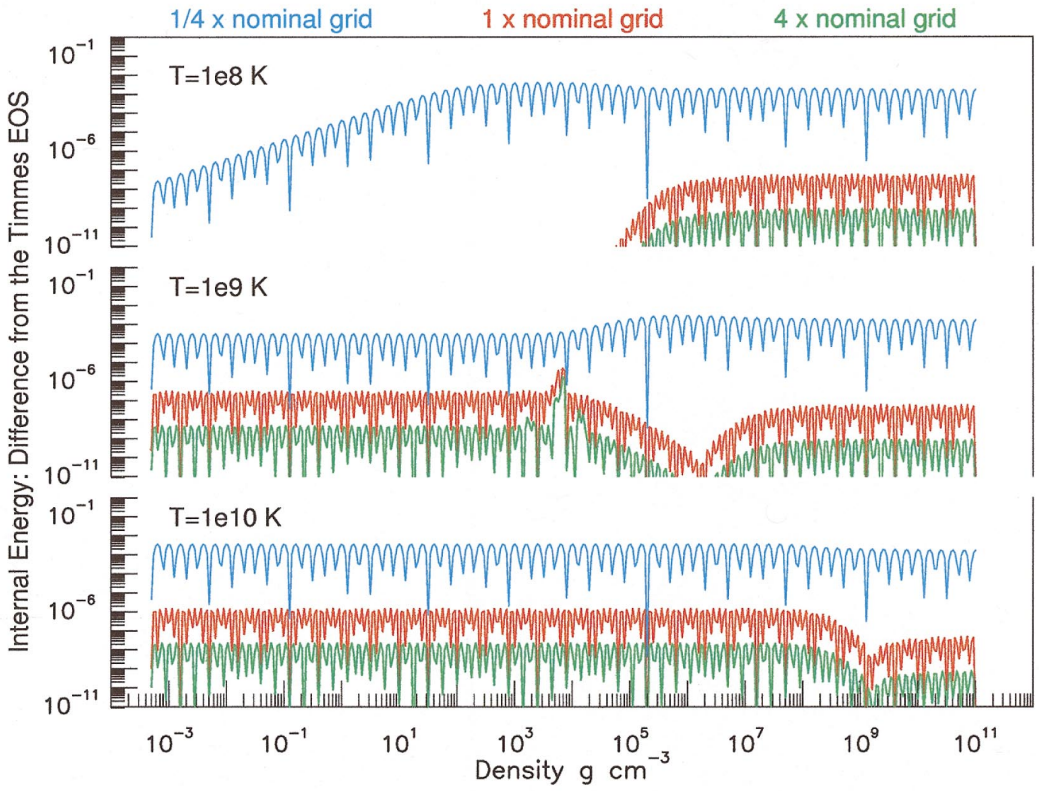

FIG. 2.—Absolute value of the relative difference from the Timmes EOS for the specific internal energy. The format is the same as in Fig. 1. Error in the specific internal energy are about 1–2 orders of magnitude smaller than the corresponding error in the pressure. The red (nominal grid) and green (4 times nominal grid) curves go below the scale of the *y*-axis in the upper panel because contributions from ions dominate the total internal energy. The blue curve, however remains on the upper panel plot because the errors in the internal energy made by using the 1/4 nominal grid are relatively large. The structure of the interpolating biquintic polynomial is clearly visible for the 1/4 nominal grid case.

orders of magnitude smaller than the corresponding error in the pressure. Like the distribution of the pressure errors, the relative error distribution the specific internal energy is relatively flat. There are, however, some regions where the relative error becomes smaller or slightly larger, such as the middle panel in Figure 2 for densities larger than about 10^3 g cm^{-3}, or the lower panel in densities larger than about 10^9 g cm^{-3}. The changes in the magnitude of the relative error are due to how well the biquintic interpolant follows the Helmholtz free energy surface, particularly as the material traverses regions where one component is decreasing (e.g., the positron contributions) and one component is increasing (e.g., electron degeneracy or radiation). The red (nominal grid) and green (4 times nominal grid) curves go below the scale of the *y*-axis in the upper panel because contributions from ions dominate the total internal energy. The blue curve, however, remains on the upper panel plot because the errors in the internal energy made by using the 1/4 nominal grid are relatively large. The structure of the interpolating biquintic polynomial is clearly visible for the 1/4 nominal grid case (*blue curves*).

The specific entropy relative to the Timmes EOS is shown in Figure 3, and the layout of the figure is the same as in Figure 1. Typical errors in the specific entropy for the three different density-temperature grids are similar to those of the typical errors in the specific internal energy and pressure, so most of analysis of Figures 1–2 applies to Figure 3 as well.

The errors made in the partial derivative of the pressure with temperature, the partial derivative of the specific internal energy with temperature, and the specific entropy with density are shown in Figures 4–6, respectively. The errors incurred when using the 4 times nominal grid are the smallest, as expected, and the error associated when the 1/4 nominal grid is used are the largest. What is more remarkable is that, in general, the derivative quantities are as precise as the integrated quantities; there is no general increase in the size of the errors even though these quantities are based on the second partial derivatives of the Helmholtz free energy. The conditions of equation (14) which were imposed on the interpolating polynomial are the primary reason for this behavior.

The locations of the sharp minima in Figures 1–6 correspond to points which happen to be near zeros of the difference from the exact EOS. Thus, the locations of the minima (there would be more of them), and the amplitudes of minima (they would be deeper) depend on the step size used in making the plots (not the step size used in constructing the table). It is the envelope of the maximum error curves that limit the accuracy, since the accuracy is perfect at the grid points. How the error changes between points of maximum error, which is almost always at half-grid points, indicates the distribution of the errors.

Figures 7–9 show the deviation made by the Timmes EOS and the Helmholtz EOS in satisfying the three thermodynamic identities of equations 2–4. The smaller the deviation, with zero being the perfect case, the closer the equation of state comes to satisfying this thermodynamic consistency relation. As asserted in § 2.1, the Helmholtz EOS satisfies thermodynamic consistency to the limiting precision of IEEE 488 64 bit arithmetic over the entire temperature-density plane under consider-

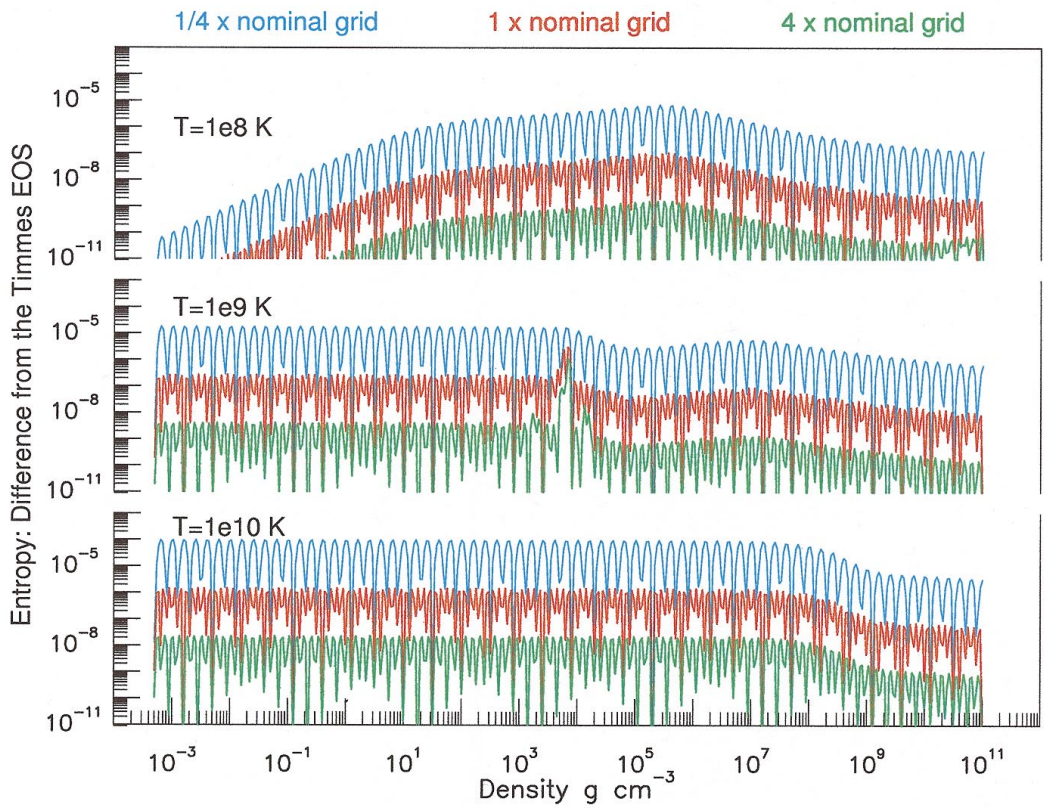

FIG. 3.—Modulus of the relative difference from the Timmes EOS for the specific entropy. The format is the same as in Fig. 1, and much of the analysis of Figs. 1 and 2 apply to the specific entropy.

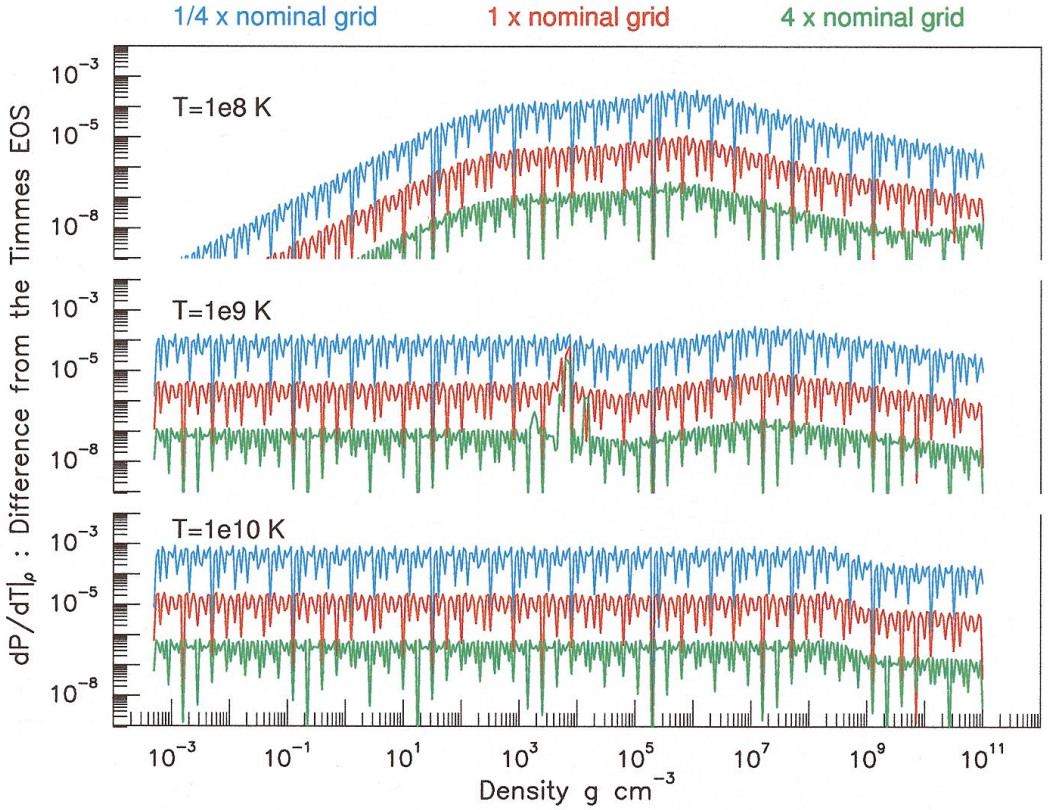

FIG. 4.—Modulus of the relative difference from the Timmes EOS for the derivative of the pressure with respect to the temperature

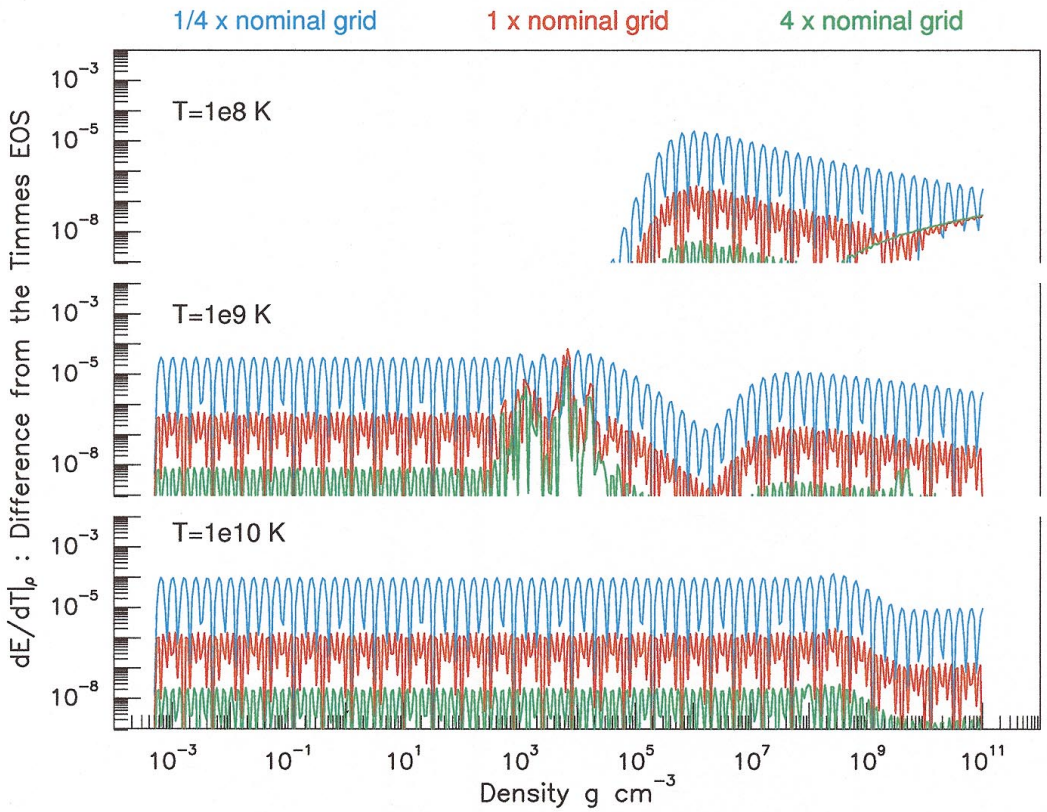

FIG. 5.—Absolute value of the relative difference from the Timmes EOS for the derivative of the specific internal energy with respect to the temperature.

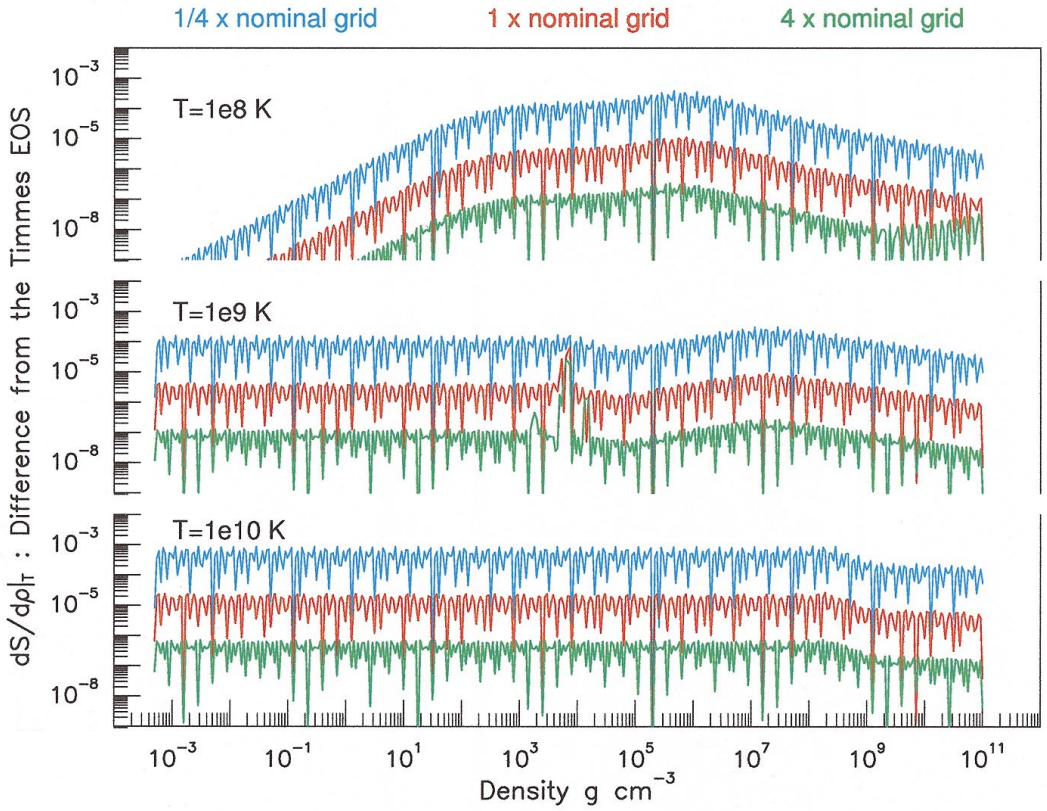

FIG. 6.—Absolute value of the relative difference from the Timmes EOS for the derivative of the specific entropy with respect to the density

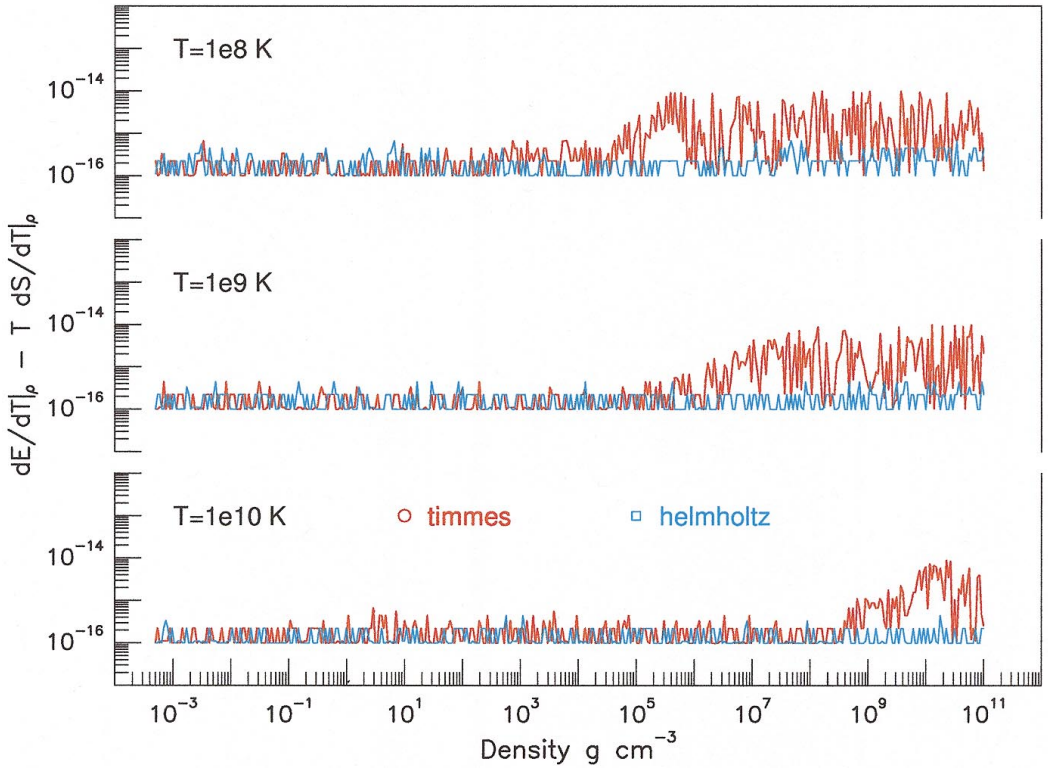

FIG. 7.—Relative difference of the thermodynamic relation $\partial E/\partial T|_\rho = T\partial S/\partial T|_\rho$ for the Timmes EOS and the Helmholtz EOS. The smaller the deviation, with zero deviation being the perfect case, the closer the equation of state comes to satisfying thermodynamic consistency.

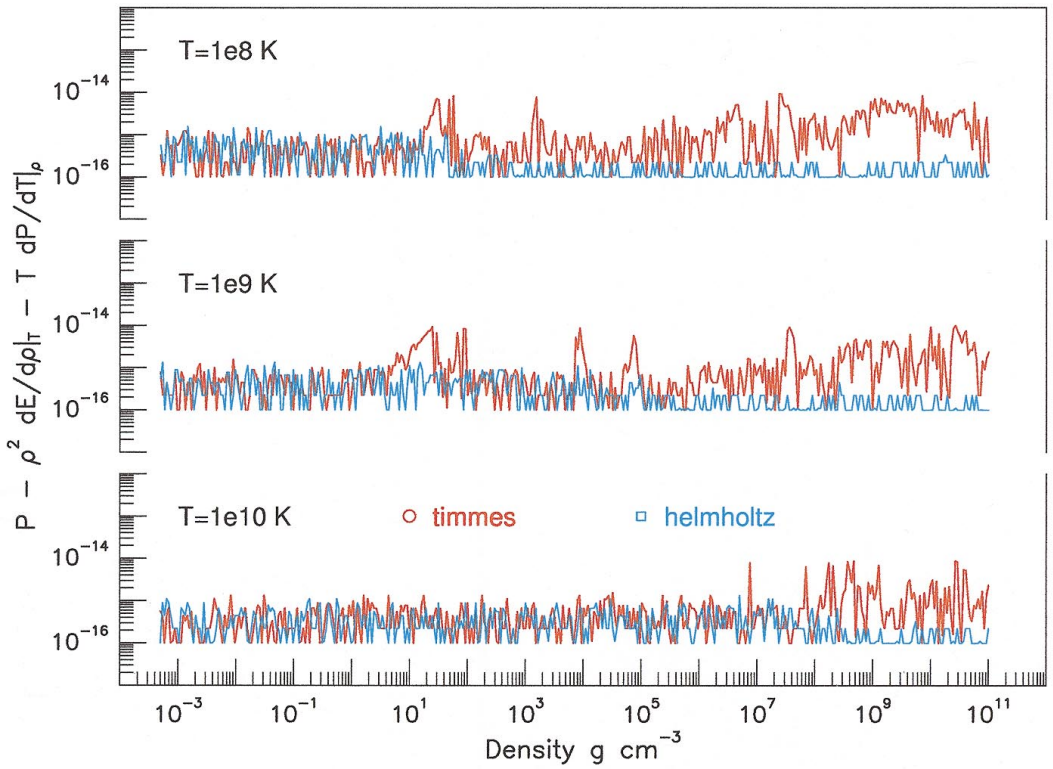

FIG. 8.—Relative difference of the thermodynamic relation $P = \rho^2\partial E/\partial\rho|_T + T\partial P/\partial T|_\rho$ for the Timmes EOS and the Helmholtz EOS

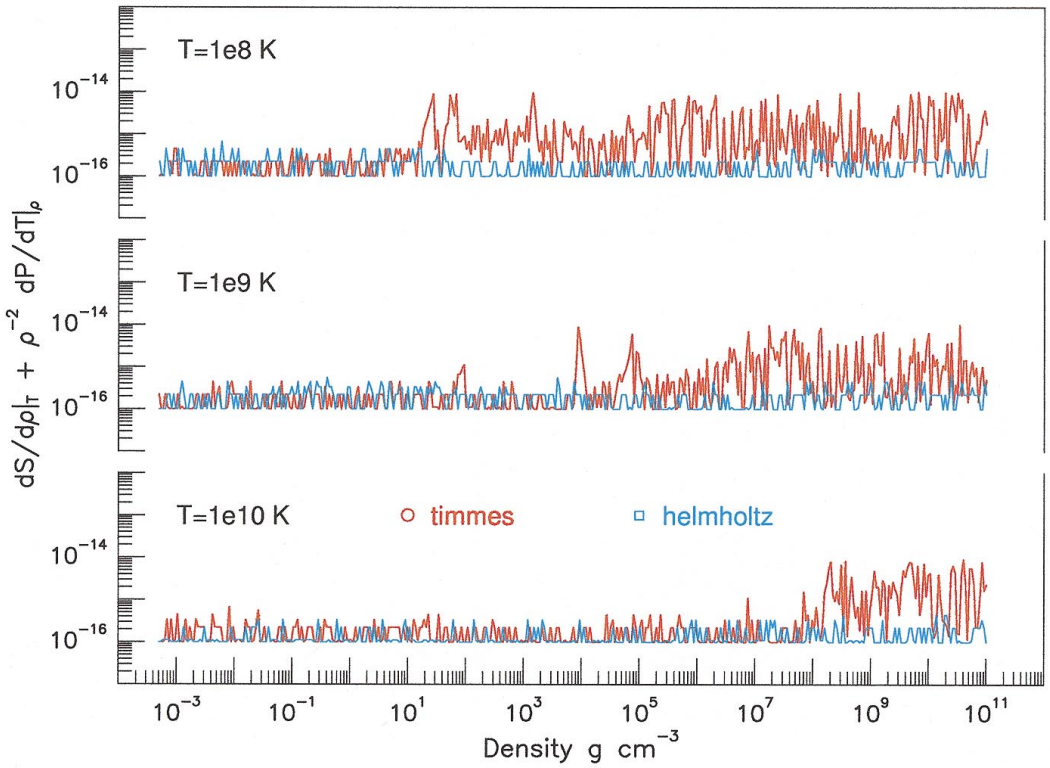

FIG. 9.—Relative difference of the thermodynamic relation $-\partial S/\partial\rho\,|_T = 1/\rho^2 \partial P/\partial T\,|_\rho$ for the Timmes EOS and the Helmholtz EOS

ation. The consistency of the Timmes EOS is quite good, but not perfect at the largest densities, because of delicate cancellations which occur in very degenerate material.

The speed of the Helmholtz EOS was evaluated in the same manner as the five EOS routines analyzed by Timmes & Arnett (1999). Briefly, the Helmholtz EOS was called 10^8 times in ordered, random, and constant entropy sweeps. An ordered sweep loops through 10^4 temperature points and 10^4 density points, both starting from the smallest value and finishing on the largest value in evenly spaced logarithmic steps. This type of sweep uniformly samples the entire temperature-density region under consideration. A random sweep chooses 10^8 arbitrary temperature and density points that are uniformly distributed. This type of sweep minimizes any speed advantage the Helmholtz EOS might gain in having the next point to be evaluated also be a nearby (in cache) point. An entropy sweep loops through 10^4 temperature and 10^4 density points, chosen in such a way that the specific entropy remains constant. This type of sweep mimics a stellar evolution calculation since most of a star's life is spent evolving at roughly constant entropy. The total CPU time spent executing each type of sweep was divided by the 10^8 calls to obtain the number of CPU seconds per call.

The Helmholtz EOS timing tests were run on five different computers; three Silicon Graphics workstations, one Sun workstation, and one LINUX PC. Each of the computers had a different CPU clock speed (195–450 MHz), bus clock speed (30–400 Mbyte s^{-1}), main memory size (64–2000 Mbyte), and cache memory size (0.032–4 Mbyte). The Helmholtz EOS routine was compiled and executed under FORTRAN 77 and FORTRAN 90. When possible, the compilation was performed with one of four different compiler option sets, from a set that requested no code optimization to a set that requested routines to be in-lined, do loops to be unrolled, and aggressive code optimization. Searches through the Helmholtz free energy table

TABLE 1

RELATIVE TIMINGS IN SERIAL MODE[a]

	TYPE OF TEMPERATURE AND DENSITY SWEEP		
EOS	Ordered	Random	Entropy
Timmes.....	106	106	106
Helmholtz.....	0.8	0.9	0.8
Arnett	1.0	1.1	1.1

[a] CPU time per call for each EOS operating in serial mode on the nominal grid. All values have been normalized to the Arnett EOS for ordered sweeps in serial mode (see Timmes & Arnett 1999 for a discussion of the tabular Arnett EOS). The table entries are generally independent of the machine architecture and compiler options used.

TABLE 2

RELATIVE TIMINGS IN PIPELINE MODE[a]

EOS	TYPE OF TEMPERATURE AND DENSITY SWEEP		
	Ordered	Random	Entropy
Timmes.....	106	106	106
Helmholtz.....	0.2	0.3	0.3
Arnett	0.4	0.5	0.5

[a] CPU time per call for each EOS operating in pipeline mode, with a pipe size of 10^4, on the nominal grid. All values have been normalized to the Arnett EOS for ordered sweeps in *serial* mode (see Timmes & Arnett 1999 for a discussion of the tabular Arnett EOS). The table entries are generally independent of the machine architecture and compiler options used.

are avoided by computing the table indices from the values of any given (T, $Y_e\rho$ pair) (i.e., the table is hashed). All divisions (which are computationally expensive) used in evaluating the table interpolants were removed, as these divisions can be computed once and then stored. The absolute speed of the Helmholtz EOS routine depends, obviously, on the machine architecture and compiler options employed. These dependences can be minimized, and meaningful comparisons made, by comparing the relative speed of the Helmholtz EOS routine. Thus, the timing results shown in Tables 1 and 2 are normalized to the Arnett EOS, which was the normalization choice in the Timmes & Arnett survey. Hence, the results of the present paper may be directly compared to the results in the Timmes & Arnett survey. Like the Helmholtz EOS, the Arnett EOS also employs a table look-up scheme for the electron-positron plasma. Timmes & Arnett give a full description of the Arnett EOS.

Table 1 shows the relative timing results when the Helmholtz EOS operates in serial mode on the nominal grid, with serial mode being defined as the EOS routine operating on a single temperature, density, and composition point. A separate call is required for each distinct input. Table 2 shows the relative timing results when the Helmholtz EOS operates in pipeline mode on the nominal grid, with pipeline mode being defined as the EOS routine operating on entire temperature, density and composition arrays. Pipeline mode rewards routines that made efficient use of the cache memory. Note, that the values in Tables 1 and 2 have been normalized to the Arnett EOS for ordered sweeps in *serial* mode, so that any advantage from operating in pipeline mode is explicit.

Tables 1 and 2 indicate that the execution speed of the Helmholtz EOS and the Arnett EOS routines increase by a factors of 2–5 when operated in pipeline mode rather than serial mode, because use of data cache memory is more efficient. This result is dependent on the size of arrays being operated on in pipeline mode. In general, the larger the array sizes, the greater the pipeline mode speed up. The results in Table 2 are for an array size of 10^4 and the nominal grid. These two EOS routines executed ordered sweeps about 30% faster than random sweeps, and about 10% faster than entropy sweeps. The chief reason for this behavior is that information for neighboring points is located next to each other in physical memory. Since ordered sweeps calculated the EOS for neighboring points and random sweeps calculate the EOS for widely scattered points, the ordered sweep is more likely than the random sweep to access data already loaded into the processor cache rather than having to access this data from the slower main memory. This reduction in the time required to access information from memory translates into a faster overall execution speed. Tables 1 and 2 show that the execution speed of the Timmes EOS is about the same in serial and pipeline modes for all sweep types. The reason for this behavior is that the Timmes EOS performs a root-find for the chemical potential in-line, which consumes the majority of the CPU time for any given temperature and density input point.

Tables 1 and 2 suggest that the Helmholtz EOS is about 10%–20% faster than the Arnett EOS, and it is worth repeating that both of these EOS routines use table lookup schemes to evaluate the electron-positron thermodynamics. The Timmes EOS, not surprisingly, is the much slower than the Helmholtz EOS routine or the Arnett EOS routine since it was designed to forsake any speed in favor of maximum accuracy.

Overall, Figures 1–9 show that the Helmholtz EOS routine achieves good accuracy with the nominal temperature-density grid, and, by design, achieves perfect thermodynamic consistency. Compared to the five EOS routines surveyed by Timmes & Arnett (1999), the Helmholtz EOS is more accurate than all but one of the EOS routines, is more thermodynamically consistent than any of the EOS routines analyzed (in some cases by an average of 8 orders of magnitude more consistent), and is faster than any of the EOS routines tested.

4. SUMMARY

An electron-positron equation of state that is based on table interpolation of the Helmholtz free energy has been developed and analyzed. The interpolation scheme guarantees perfect thermodynamic consistency (Figs. 7–9), independent of the interpolating function. The particular interpolating function developed in § 2.2, a biquintic Hermite polynomial, faithfully reproduces the underlying Helmholtz free energy data in the table (Figs. 1–3) and yields derivatives of the pressure, specific entropy, and specific internal energy that are smooth and continuous (Figs. 4–6). The resulting Helmholtz EOS is generally more accurate, more thermodynamically consistent, and executes faster (Tables 1 and 2) than any of the five EOS routines examined in the Timmes & Arnett survey. This suggests that when an optimal balance of accuracy, thermodynamic consistency, and speed is desirable, then the Helmholtz EOS is an excellent choice, particularly for multidimensional models of stellar phenomena.

F.X.T. thanks the members and affiliates of the Center on Astrophysical Thermonuclear Flashes for incinerating discussions.

This work is supported by the Department of Energy under grant B341495 to the Center on Astrophysical Thermonuclear Flashes at the University of Chicago (F.X.T.), and by NASA under ATP grants NAG5-3099 and CAN No. S5-153 (F.D.S.).

APPENDIX A

THERMODYNAMICALLY CONSISTENT INTERPOLATION SUBROUTINE

A FORTRAN subroutine that implements the thermodynamically consistent, biquintic Hermite interpolation scheme for an electron-positron plasma is given below. Note the scaling with Y_e; so that a two-dimensional table of the Helmholtz free energy $F(\rho, T)$ constructed for $Y_e = 1$ (pure hydrogen) is valid for any composition. Some execution efficiency has been sacrificed in order to gain clarity or shorten the printed length. An example of this inefficiency are multiple divisions which occur could be computed once and stored. Another inefficiency is storing the Helmholtz free energy and its eight derivatives in separate arrays; storing the nine points sequentially in an array generally results in more efficient use of cache memory. Finally, the main table lookup could be done only once instead of the six times as done below; this will further improve the cache hit rate.

```
        subroutine tcteos(temp,den,ye,
       1                      ptot,etot,stot,dpdd,dpdt,dedd,dedt,dsdd,dsdt)
        implicit none
        save

c..
c..this routine performs a thermodynamically consistent interpolation
c..in a tabular electron-positron equation of state using biquintic
c..hermite basis functions.
c..
c..input:
c..temp = temperature(in K)
c..den = density (in g cm^-3)
c..ye = electrons per baryon = zbar/abar
c..
c..also input through a common block is the table of the helmholtz
c..free energy and eight of its partial derivatives:
c..f, df_d, df_t, df_dd, df_tt, df_dt, df_ddt, df_dtt and df_ddtt
c..
c..output:
c..ptot = pressure (ergs cm^-3)
c..etot = specific internal energy (ergs g^-1)
c..stot = specific entropy (ergs g^-1 K^-1)
c..dpdd = partial derivative of pressure with density (ergs g^-1)
c..dpdt = partial derivative of pressure with temperature (ergs cm^-3 K^-1)
c..dedd = partial derivative of energy with density (ergs cm^-3 g^-2)
c..dedt = partial derivative of energy with temperature (ergs g^-1 K^-1)
c..dsdd = partial derivative of entropy with density (ergs cm^-3 g^-2 K^-1)
c..dsdt = partial derivative of entropy with temperature (ergs g^-1 K^-2)
c..
c..declare the pass
        double precision temp,den,ye,ptot,etot,stot,dpdd,dpdt,dedd,dedt,
       1 dsdd,dsdt

c..declare the internal variables
        integer i,j,iat,jat
        double precision tlo,thi,tstp,tstpi,dlo,dhi,dstp,dstpi,
       1 tsav,dsav,free,df_d,df_t,df_dd,df_tt,df_dt,dt,dt2,dti,dt2i,dd,
       2 dd2,ddi,dd2i,xt,xd,mxt,mxd,si0t,si1t,si2t,si0mt,si1mt,si2mt,si0d,
       3 si1d,si2d,si0md,si1md,si2md,dsi0t,dsi1t,dsi2t,dsi0mt,dsi1mt,
       4 dsi2mt,dsi0d,dsi1d,dsi2d,dsi0md,dsi1md,dsi2md,ddsi0t,ddsi1t,
       5 ddsi2t,ddsi0mt,ddsi1mt,ddsi2mt,ddsi0d,ddsi1d,ddsi2d,ddsi0md,
       6 ddsi1md,ddsi2md,z,psi0,dpsi0,ddpsi0,psi1,dpsi1,ddpsi1,psi2,dpsi2,
       7 ddpsi2,w0t,w1t,w2t,w0mt,w1mt,w2mt,w0d,w1d,w2d,w0md,w1md,w2md,
       8 din,herm5
```

```
c..the coefficient arrays have been read in elsewhere, bring them in
c..through a common block communication. the array d(1:imax) holds the
c..density grid points, and t(1:jmax) holds the temperature grid points.
c..change imax and jmax to whatever size the table might be.
        integer imax,jmax
        parameter (imax = 100, jmax = 50)
        double precision d(imax),t(jmax)
        double precision f(imax,jmax),fd(imax,jmax),ft(imax,jmax),
       1 fdd(imax,jmax),ftt(imax,jmax),fdt(imax,jmax),fddt(imax,jmax),
       2 fdtt(imax,jmax),fddtt(imax,jmax)
        common /htable/ f,fd,ft,fdd,ftt,fdt,fddt,fdtt,fddtt

c..quintic hermite basis statement functions
c..psi0 and its derivatives
        psi0(z) = z**3 * ( z * (-6.0d0*z + 15.0d0)-10.0d0) + 1.0d0
        dpsi0(z) = z**2 * ( z * (-30.0d0*z + 60.0d0)-30.0d0)
        ddpsi0(z) = z* ( z * (-120.0d0*z + 180.0d0)-60.0d0)

c..psi1 and its derivatives
        psi1(z) = z* ( z**2 * ( z * (-3.0d0*z + 8.0d0)-6.0d0) + 1.0d0)
        dpsi1(z) = z*z * ( z * (-15.0d0*z + 32.0d0)-18.0d0) + 1.0d0
        ddpsi1(z) = z * ( z * (-60.0d0*z + 96.0d0)-36.0d0)

c..psi2 and its derivatives
        psi2(z) = 0.5d0*z*z*(z * (z* (-z + 3.0d0)-3.0d0) + 1.0d0)
        dpsi2(z)= 0.5d0*z*(z *(z*(-5.0d0*z + 12.0d0)-9.0d0) + 2.0d0)
        ddpsi2(z) = 0.5d0*(z* (z* (-20.0d0*z + 36.0d0)-18.0d0) + 2.0d0)

c..bicubic hermite polynomial statement function
        herm5(i,j,w0t,w1t,w2t,w0mt,w1mt,w2mt,w0d,w1d,w2d,w0md,w1md,w2md)=
       1      f(i,j) *w0d*w0t + f(i+1,j) *w0md*w0t
       2     +f(i,j+1) *w0d*w0mt + f(i+1,j+1) *w0md*w0mt
       3     +ft(i,j) *w0d*w1t + ft(i+1,j) *w0md*w1t
       4     +ft(i,j+1) *w0d*w1mt + ft(i+1,j+1) *w0md*w1mt
       5     +ftt(i,j) *w0d*w2t + ftt(i+1,j) *w0md*w2t
       6     +ftt(i,j+1) *w0d*w2mt + ftt(i+1,j+1) *w0md*w2mt
       7     +fd(i,j) *w1d*w0t + fd(i+1,j) *w1md*w0t
       8     +fd(i,j+1) *w1d*w0mt + fd(i+1,j+1) *w1md*w0mt
       9     +fdd(i,j) *w2d*w0t + fdd(i+1,j) *w2md*w0t
       &     +fdd(i,j+1) *w2d*w0mt + fdd(i+1,j+1) *w2md*w0mt
       1     +fdt(i,j) *w1d*w1t + fdt(i+1,j) *w1md*w1t
       2     +fdt(i,j+1) *w1d*w1mt + fdt(i+1,j+1) * w1md*w1mt
       3     +fddt(i,j) *w2d*w1t + fddt(i+1,j) *w2md*w1t
       4     +fddt(i,j+1) *w2d*w1mt + fddt(i+1,j+1) *w2md*w1mt
       5     +fddtt(i,j) *w1d*w2t + fdtt(i+1,j) *w1md*w2t
       6     +fdtt(i,j+1) *w1d*w2mt + fdtt(i+1,j+1) *w1md*w2mt
       7     +fddtt(i,j) *w2d*w2t + fddtt(i+1,j) *w2md*w2t
       8     +fddtt(i,j+1) *w2d*w2mt + fddtt(i+1,j+1)*w2md*w2mt

c..find the table locations, entering with ye * density
c..change the jat and iat lines if the table is not hashed in log space
        jat = int((log10(temp) - tlo)/tstp) + 1
        din = ye * den
        iat = int((log10(din) - dlo)/dstp) + 1

c..various differences
        dt = t(jat+1) - t(jat)
        dt2 = dt * dt
        dd = d(iat+1) - d(iat)
        dd2 = dd * dd
        xt = max((temp - t(jat))/dt, 0.0d0)
        xd = max((din - d(iat))/dd,0.0d0)
        mxt = 1.0d0 - xt
```

```
        mxd = 1.0d0 - xd

c..evaluate the basis functions
         si0t = psi0(xt)
         si1t = psi1(xt)*dt
         si2t = psi2(xt)*dt2

         si0mt = psi0(mxt)
         si1mt = -psi1(mxt)*dt
         si2mt = psi2(mxt)*dt2

         si0d = psi0(xd)
         si1d = psi1(xd)*dd
         si2d = psi2(xd)*dd2

         si0md = psi0(mxd)
         si1md = -psi1(mxd)*dd
         si2md = psi2(mxd)*dd2

c..and their first derivatives
         dsi0t = dpsi0(xt)/dti
         dsi1t = dpsi1(xt)
         dsi2t = dpsi2(xt)*dt

         dsi0mt = -dpsi0(mxt)/dt
         dsi1mt = dpsi1(mxt)
         dsi2mt = -dpsi2(mxt)*dt

         dsi0d = dpsi0(xd)/dd
         dsi1d = dpsi1(xd)
         dsi2d = dpsi2(xd)*dd

         dsi0md = -dpsi0(mxd)/dd
         dsi1md = dpsi1(mxd)
         dsi2md = -dpsi2(mxd)*dd

c..and their second derivatives
         ddsi0t = ddpsi0(xt)/dt2
         ddsi1t = ddpsi1(xt)/dt
         ddsi2t = ddpsi2(xt)

         ddsi0mt = ddpsi0(mxt)/dt2
         ddsi1mt = -ddpsi1(mxt)/dt
         ddsi2mt = ddpsi2(mxt)

         ddsi0d = ddpsi0(xd)/dd2
         ddsi1d = ddpsi1(xd)/dd
         ddsi2d = ddpsi2(xd)

         ddsi0md = ddpsi0(mxd)/dd2
         ddsi1md = -ddpsi1(mxd)/dd
         ddsi2md = ddpsi2(mxd)

c..the free energy
         free = herm5(iat,jat,
       1           si0t,si1t,si2t,si0mt,si1mt,si2mt,
       2           si0d,si1d,si2d,si0md,si1md,si2md)

c..derivative of the free energy with density
         df_d = herm5(iat,jat,
       1           si0t,si1t,si2t,si0mt,si1mt,si2mt,
       2           dsi0d,dsi1d,dsi2d,dsi0md,dsi1md,dsi2md)

c..derivative of the free energy with temperature
```

```
         df_t = herm5(iat,jat,
        1           dsi0t,dsi1t,dsi2t,dsi0mt,dsi1mt,dsi2mt,
        2           si0d,si1d,si2d,si0md,si1md,si2md)

c..second derivative free energy with to density^-2
         df_dd = herm5(iat,jat,
        1           si0t,si1t,si2t,si0mt,si1mt,si2mt,
        2           ddsi0d,ddsi1d,ddsi2d,ddsi0md,ddsi1md,ddsi2md)

c..second derivative of the free energy with temperature^-2
        df_tt = herm5(iat,jat,
        1           ddsi0t,ddsi1t,ddsi2t,ddsi0mt,ddsi1mt,ddsi2mt,
        2             si0d,si1d,si2d,si0md,si1md,si2md)

c..second derivative of the free energy with to temperature and density
        df_dt = herm5(iat,jat,
        1           dsi0t,dsi1t,dsi2t,dsi0mt,dsi1mt,dsi2mt,
        2           dsi0d,dsi1d,dsi2d,dsi0md,dsi1md,dsi2md)

c..set the return arguments; the electron-positron
c..pressure, specific entropy, and internal energy
c..along with their partial derivatives
         ptot = din^-2 * df_d
         dpdt = din^-2 * df_dt
         dpdd = ye * (din^-2 * df_dd + 2.0d0 * din * df_d)

         stot = -df_t * ye
         dsdt = -df_tt * ye
         dsdd = -df_dt * ye^-2

         etot = ye * free + temp * stot
         dedt = temp * dsdt
         dedd = ye^-2 * df_d + temp * dsdd
         return
         end
```

REFERENCES

Aparicio, J. M. 1998, ApJS, 117, 627

Arnett, D. 1996. Supernovae and Nucleosynthesis: an Investigation of the History of Matter, from the Big Bang to the Present (Princeton: Princeton Univ. Press)

Blinnikov, S. I., Dunina-Barkovskaya, N. V., & Nadyozhin, D. K. 1996, ApJS, 106, 171

———. 1998, ApJS, 118, 603

Cohen, E. R., & Taylor, B. N. 1987, J. Res. NBS, 92, 2

Costantini, P., & Manni, C. 1996, Comp. Aided Geom. Design, 13, 307

Davis, P. J. 1963, Interpolation and Approximation (Waltham: Blaisdell)

Iben, I., Jr., Fujimoto, M. Y., & MacDonald, J. 1992, ApJ, 388, 521

Nadyozhin, D. K. 1974, Nauchnye informatsii Astron., Sov. USSR, 32, 3, 33, 117

Press, W. H., Teukolsky, S. A., Vetterling, W. T., & Flannery, B. P. 1996, Numerical Recipes in FORTRAN 90 (Cambridge: Cambridge Univ. Press)

Reif, F. 1965, Fundamentals of Statistical and Thermal Physics (New York: McGraw-Hill)

Späth, H. 1995, One Dimensional Spline Interpolation Algorithms (Wellesley: A. K. Peters)

Swesty, D. 1996, J. Comp. Phys., 127, 118

Timmes, F. X., & Arnett, D. 1999, ApJS, 125, 294

Weaver, T. A., Zimmerman, G. B., & Woosley, S. E. 1978, ApJ, 225, 1021